



Study on Large Deformation Mechanism of Roadway with Close and Multi Coal Seam in Mining

Yongsheng Bao · Dongfang Su · Hongwei Mu

Received: 13 October 2019 / Accepted: 4 October 2020 / Published online: 11 October 2020
© Springer Nature Switzerland AG 2020

Abstract In view of the serious local deformation of roadway in close coal seam mining, the seismic computed tomography (CT) and spatio-temporal evolution of microseismic were comprehensively investigated in this study. The static coal load and dynamic load disturbance were used to reveal the local large deformation mechanism of the mining roadway with coal pillars in close and multi coal seams. The result of this study showed that CT could accurately detect the static load stress concentration area, which was mainly located in the zone that was comprehensively influenced by overlying coal pillars, side abutment pressure, and pilot support pressure. The overlying coal pillar was the main influencing factor. In the Xinzhouyao mine, the static load stress concentration area detected by CT and the dynamic load disturbance concentration area detected by the microseismic spatio-temporal law were consistent with the roadway

deformation position. According to the comprehensive theoretical model study, the main influencing factors of the local large deformation of the roadway were the static load stress concentration caused by the overlying coal pillar and the dynamic load disturbance caused by the fracture and slippage of the overlying coal pillar and roof under the influence of mining. The superposition of dynamic load disturbance and static load concentrated stress caused large deformation of the roadway, of which the static load stress concentration was the main influencing factor. The conclusions of this study can guide the determination of the risk zone of rock burst under similar conditions.

Keywords Multi-coal mining · Coal pillar · Large deformation of roadway · Microseismic monitoring · Seismic computed tomography CT

Y. Bao
Datong Coal Mine Group Co., Ltd., Datong 037003,
Shanxi, China

D. Su (✉) · H. Mu
School of Civil and Resource Engineering, University of
Science and Technology Beijing, Beijing 100083, China
e-mail: 1356133041@qq.com

D. Su · H. Mu
State Key Laboratory of the Ministry of Education of
China for High-Efficient Mining and Safety of Metal
Mines, University of Science and Technology Beijing,
Beijing 100083, China

1 Introduction

Large deformation of roadways has always been a critical issue affecting the safety production of the coal mine, which it is generally believed that it will only occur in deep soft rock roadways. However, with the development of multi-coal mining, large deformation phenomena were observed in the roadway when the lower coal seam was mined in shallow coal seams (Gao 2018), and rock burst might be triggered in localized areas (Zhao 2018; Sun 2019). The number of

long-wall mining coal mines in China and around the world is increasing rapidly (Mark 2007; Cartwright 1997; Tulu 2018). Therefore, it is urgent to study the mechanism of large deformation of roadway with coal pillars in close coal seam mining.

At present, the research on the large deformation of roadway is mainly focused on deep and single coal seam mining. The deformation mechanism of deep soft rock roadway has been studied from the perspectives of theory (Yang 2013; Qing-bin 2013), numerical simulation (Chen 2011; Yang 2017), similar material simulation (Li 2015), and field measurement (Li 2019). The measures to control the deformation of deep soft rock roadway have been also studied (Wang 2017; Yan 2012; Liu 2018). These theories and practices have accelerated the study of the deformation mechanism of roadways. However, for the first coal seam to be mined, the vertical and horizontal stress components at any given depth are generally considered to be relatively uniform in the mine zone, and the fracture of the roof is also periodic. In addition, the deformation of the roadway is very common throughout the roadway. Close and multi-coal seam refers to that the upper coal seam mining can produce pressure relief, stress concentration and secondary dynamic load disturbance to the lower coal seam. The stress and roof fracture pattern are not consistent with the single coal seam when mining the lower coal seam in close multiple coal seams, which is closely related to the coal seam structure under the condition of close multi-coal seams mining. Therefore, the mechanism of large deformation of deep soft rock roadway cannot fully explain the large deformation of roadway caused by coal mining in the shallow multi-coal seam with coal pillars.

In recent years, many scientists have conducted a series of fruitful research on roadway deformation and mine pressure induced by coal pillars under multi-coal mining conditions. Jiang Fuxing () concluded that the stress concentration caused by the overlying coal pillars was an important cause of the instability of the lower coal seam by conducting stress analysis on the coal pillars in multi-coal mining. Wang Cunwen (2009) put forward that the coal pillar was the fundamental cause of induced impact deformation via the establishment of the structural mechanics model of island coal pillars. Focusing on the dynamic strata pressure caused by coal pillar, Ju jinfeng (2010) analyzed the stability of key block structure above the

coal pillar and combined similar simulation experiments, concluded that the failure of the lower key block caused by the instability of the three-hinged structure above the coal pillar was the main reason for the dynamic load pressure. Regarding the dynamic strata pressure caused by the small coal pillars left by the room mining, Zhu (2017) believed that the stress caused by the instability of large-area small coal pillars caused by the rotation of the critical layer of the coal pillars was the main reason for the occurrence of dynamic strata pressure by experiment and numerical simulation. These studies provide a reference for revealing the mechanism of roadway deformation and rock burst caused by mining coal pillars in close multiple coal seam.

In summary, previous studies focused on the stress distribution law and the roadway deformation mechanism of coal pillars in close multiple coal seams but the mechanism of large deformation of coal roadway from the perspective of static stress concentration and dynamic disturbance is still remaining to be researched. According to the inversion results of on-site seismic computed tomography CT and the microseismic temporal-spatial evolution, the large deformation law of roadway was studied from the perspectives of static load stress concentration and dynamic strata disturbance. The theoretical model of roadway deformation in coal mining with close multiple coal seams was summarized, which reveals the mechanism of large deformation of roadway in coal mining with close multiple coal seams.

2 Project Overview

The Xinzhouyao mine is located in the Datong mining area of Shanxi Province with a primary mineable coal bed of Jurassic coal seam. From the top to bottom, the main mining coal bed consists of 9, 11, and 14 # coal seams with a buried depth of 100–300 m and a coal seam spacing of 8–30 m, which is a typical close multi-coal seam mine. In the eastern second and third panel districts of Xinzhouyao mine, the 11 and 14 # coal seams overlap, and a large number of irregular coal pillars are left during the 11-2 # coal seam mining process. Influenced by the remaining coal pillars in 11-2 # coal seam, the deformation of the lower roadway in 14-3 # coal seam is very serious, especially in the very busy working faces of 8312, 8310

and 8308 in 14-3 # coal seam. In this work, the 8308 working face was selected as the research object.

The 8308 working face is located in the 14-3 # coal seam of the eastern panel district of Xinzhouyao mine with a nearly horizontal seam dip angle and a depth of about 285 m. The top and bottom plates of the working face are hard rock. The drilling column is shown in Fig. 1. Two lanes were installed 8308 working face, including 5308 track lane and 2308 belt lane, in which the working surface was 883.57 m long and 131 m wide. The west side of the lanes was the 8310 goaf while the east side was the 8306 working face, and the section coal pillar was 20 m wide. The working face was about 30 m away from the 11-2 # coal seam. The mining of 11-2 # coal seam was completed, and the remained overlying coal pillars that affect the 8308 working face were numbered. The arrangement of 8308 working face and distribution of pillars are shown in Fig. 2.

There was no obvious deformation in the belt lane during the roadway excavation of the 8308 working face, whereas the displacement of roadway sides and floor heave of roadway were observed in the track

lane. When the track lane passed through the M1 and M2 areas during the excavation, the deformation of the roadway was more severe. The maximum displacement of roadway sides reached more than 2 m, and the single pillar reached 0.6 m at the deepest point of the bottom coal. At the scene, the deformation area of the track lane was repaired and expanded in time. However, when the M1 and M2 areas were mined from the working face, secondary deformation occurred in the track lane with a potential rock burst.

The SOS microseismic monitoring system was employed in Xinzhouyao mine, which accumulated a large amount of microseismic data during the mining on the 8308 working face. Through the deep analysis of microseismic monitoring data, the law of static load stress and dynamic load disturbance can be studied by the seismic computed tomography CT stress detection and the spatiotemporal evolution law of microseismic events, respectively, by which the large deformation mechanism of roadway in coal mining with close coal seam can be revealed.

3 Analysis of Large Deformation, Static Load Stress, and Dynamic Load Disturbance of Roadway

3.1 Static Stress Detection of the CT Technology

The seismic computed tomography CT technology is based on the microseismic monitoring data. The tomographic imaging technique is used to obtain the wave velocity in the inversion region of the working surface (Pan Junfeng 2014; Hosseini 2012). The seismic computed tomography CT technology has the advantages of advanced detection and large-scale detection, it has been widely used in the detection of stress concentration areas and the assessment of the risk of rock burst (Cao 2016; Cai 2014). The static load stress concentration region is detected by the coupling relationship between the stress and the longitudinal wave velocity (Cao 2015; Wu 2016). The positive anomaly coefficient of the longitudinal wave velocity in this region is positively correlated with the stress. The calculation formula is shown in the following Eq. (1) (Dou Lin-ming 2014). The correlation between the positive velocity coefficient and the stress concentration is shown in Table 1. The following is the mining of the seismic computed tomography detection

| Column | Lithology | Depth/m | Thickness /m |
|--------|------------------|---------|--------------|
| | Sandstone | 262.42 | 4.28 |
| | Sandstone | 266.70 | 9.53 |
| | Sandy shale | 276.23 | 2.60 |
| | 11-2# coal seam | 278.83 | 4.48 |
| | Sandstone | 283.31 | 7.8 |
| | Shale | 291.11 | 10.05 |
| | Medium sandstone | 301.16 | 5.72 |
| | Sandy shale | 306.88 | 3.20 |
| | 14-2# coal seam | 310.08 | 3.30 |
| | Sandy shale | 313.38 | 4.35 |
| | Medium sandstone | 317.73 | 5.68 |
| | 15# coal seam | 323.41 | 6.09 |
| | Sandstone | 329.50 | 1.63 |
| | Sandy shale | 331.13 | 5.15 |

Fig. 1 Column of coal and rock layers

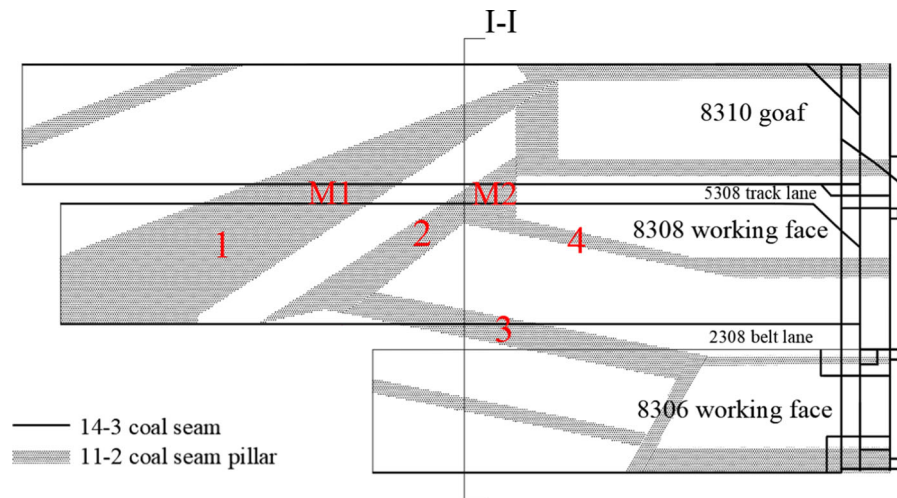


Fig. 2 Sketch map of 8308 working face and overlying pillars

Table 1 The relation between positive anomalies of wave velocity and stress concentration

| Indicators of rock burst | Characteristics of stress concentration | Positive anomalies of wave velocity A_n |
|--------------------------|---|---|
| 0 | No | < 0.05 |
| 1 | Mild | 0.05–0.15 |
| 2 | Moderate | 0.15–0.25 |
| 3 | Strong | > 0.25 |

law of the 8308 working surface, which can be used to study the main control factors of the large deformation of the roadway under similar conditions.

$$A_n = \frac{V_p - V_p^z}{V_p^z} \quad (1)$$

wherein V_p and V_p^z represent the P wave velocity value of a certain point in the inversion region and the average value of the model wave velocity, respectively.

The M1 and M2 areas with serious deformation of the actual roadway in the 8308 working face were selected as the research objects, and the inversions of microseismic data before and after the mining in these areas were performed. Specifically, the mining date 76 s of M1 and M2 areas were from December 5, 2017, to January 18, 2018, and February 5 to 28, 2018, respectively. Figure 3 shows the anomaly coefficient distribution of wave velocity obtained by the seismic computed tomography CT technique.

Before the working face moved into the M1 area, a large area of stress concentration appeared under the coal pillar 1 within 100 m in front of the working face. The positive anomaly coefficient of wave velocity reached 0.2 near the adjacent roadway, which is consistent with the large deformation area of the actual roadway. As the working faces moved forward to the position shown in Fig. 3b, the stress concentration region moved forward at the same time with an occurrence of a stress concentration region near the coal pillar 2. According to Fig. 3a–c, the vicinity of the M2 region was in a state of stress concentration for a long time. When the working face was 50 m from the M2 area, the positive anomaly coefficient of the wave velocity reached 0.2 with severe deformation. At the same time, a small-scale stress concentration occurred at the junction area between the coal pillar 3 and the 2308 track lane, indicating that the concentrated coal pillar is a high-stress concentration region. During the mining of the M2 area, a large stress concentration area appeared near the gob-side roadway within 150 m ahead, as shown in Fig. 3d. As the 8308 working face was gradually approaching the stop line, the stress concentration area tended to shift to the east side 8306 working face, but still appeared in the area adjacent to the coal pillar.

By summarizing the characteristics of the above patterns, it can be seen that the coal pillars in the working face are mostly in stress concentration zones. In addition, the stress concentration of the roadway near gob is more obvious than that of the other

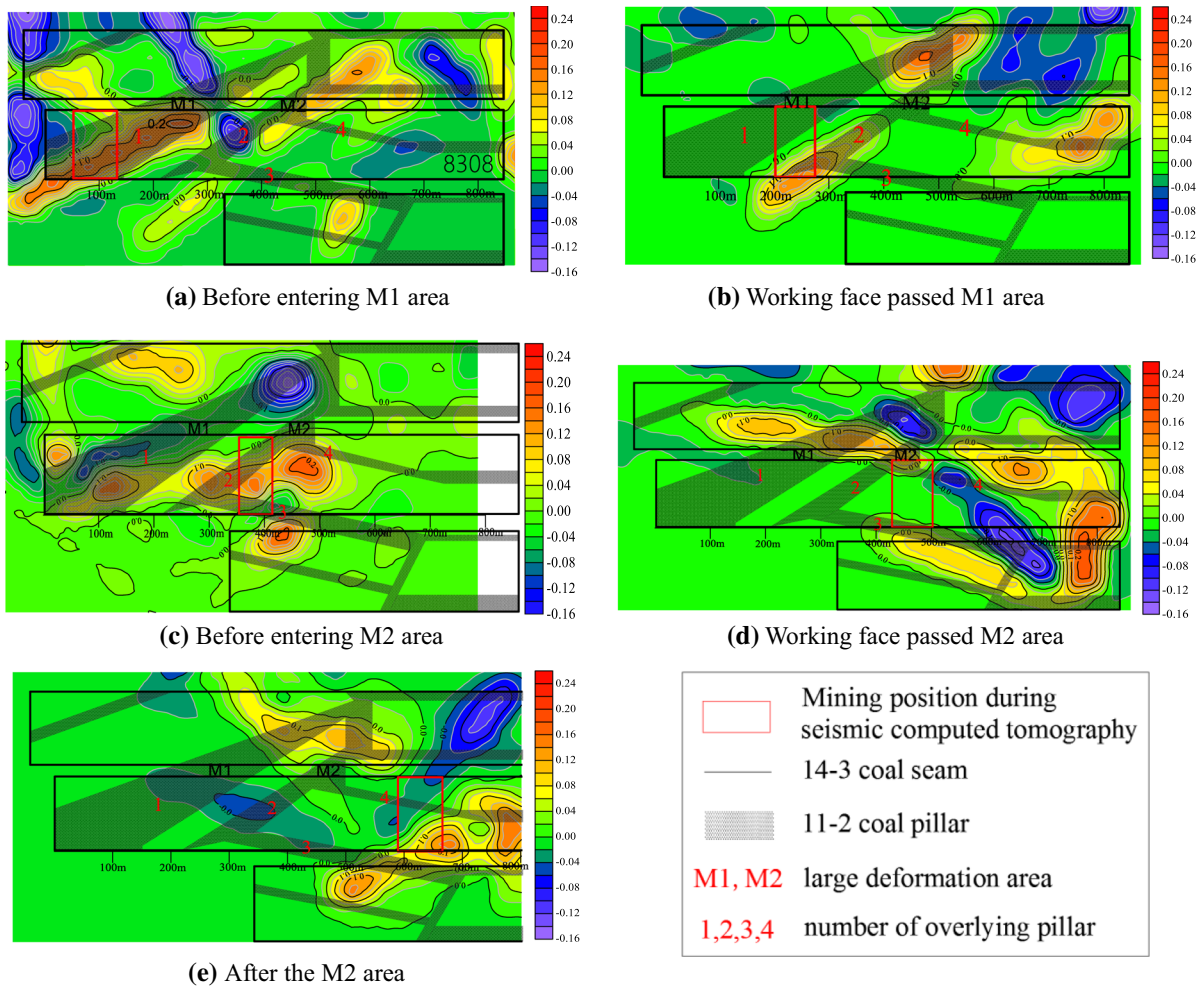


Fig. 3 Distribution of wave velocity anomaly coefficient with different mining positions

roadway. The stress concentration state changed dynamically with the advancement of the working face. At the same time, the area where the positive velocity coefficient of the wave velocity exceeded 0.2 corresponded to the large deformation area of the actual roadway.

3.2 Dynamic Load Disturbance Monitoring

Studies have shown that dynamic disturbance had an important influence on large deformation of working face and strata behaviors (Li 2017, 2018). The microseismic monitoring system can conduct real-time monitoring of microseismic events in the entire mine and automatically record microseismic activities. Source location, time and energy of microseismic

events can be calculated at the same time. Provide a basis for evaluating the degree of danger of strong mineral pressure in the whole mine. High energy mine earthquake event was a key indicator to evaluate high-intensity dynamic load disturbance (He Xueqiu 2018). According to the risky region of static stress concentration obtained by seismic computed tomography CT inversion, the dynamic disturbance was studied from the perspective of spatial positioning of microseismic data and evolution law of energy frequency.

3.2.1 Microseism Spatial Distribution Law

The original microseismic data ($> 1 \times 10^4$ J) during the entire mining period of 8308 was divided into different orders of magnitude for positioning research

in three-dimensional space. Figure 4a, b shows the plane location map of the microseismic event and the vertical profile map along the 8308 working surface.

It can be seen from Fig. 4 that the distribution of microseismic events on the horizontal section showed a zoning phenomenon, which is concentrated in the vicinity of the coal pillars and roadways near gob. The most obvious occurrence of microseismic events released energy above 10^5 J. On the striking profile, the microseismic events mainly occurred in the 14-3 and 11-2 # coal seam roofs. The statistics of microseismic events with various orders of magnitude occurring in different horizons are shown in Table 2. According to the analysis, the high energy events ($> 10^4$ J) in 14-3 # coal seam floor, 14-3 # coal roof, and 11-2 # coal roof accounted for 16, 43, and 41%, respectively. This result indicated that the microseismic event mainly occurred on the roofs of 14-3 # coal seam and 11-2 # coal seam. The microseismic events on the south side of the M2 area were mainly distributed on the 11-2 # coal seam roof, while the microseismic events on the north side of the M2 area were distributed on the 11-2 # coal seam roof and the

14-3 # coal seam roof with a predominance on the 14-3 # coal seam roof.

According to the above analysis, it was found that the microseismic event was closely related to the remaining coal pillars in the overlying coal seam, and the microseismic events mainly occurred in the 14-3 and 11-2 # coal seam roofs. Therefore, the microseismic events were stratified and screened for analysis, which were 11-2 and 14-3# coal seams and roofs. The distribution law of microseismic events during the M1 and M2 mining periods, as well as the distribution rules of the 14-3 and 11-2# coal seam roofs, were analyzed. The spatial positioning results are shown in Fig. 5.

During the M1 mining period, the microseismic events were mainly concentrated under the coal pillar 1 and near the front of the coal pillar 2. Some microseismic events were also distributed under the coal pillar in the 8310 goaf. Comparing Fig. 5c and d, the microseismic events were mainly distributed in the vicinity of the coal pillars of the 11-2 # coal seam and roof. Most of the microseismic events with more than 1×10^5 J occurred in front of the M1 area. At the same time, compared the roadways on both sides of

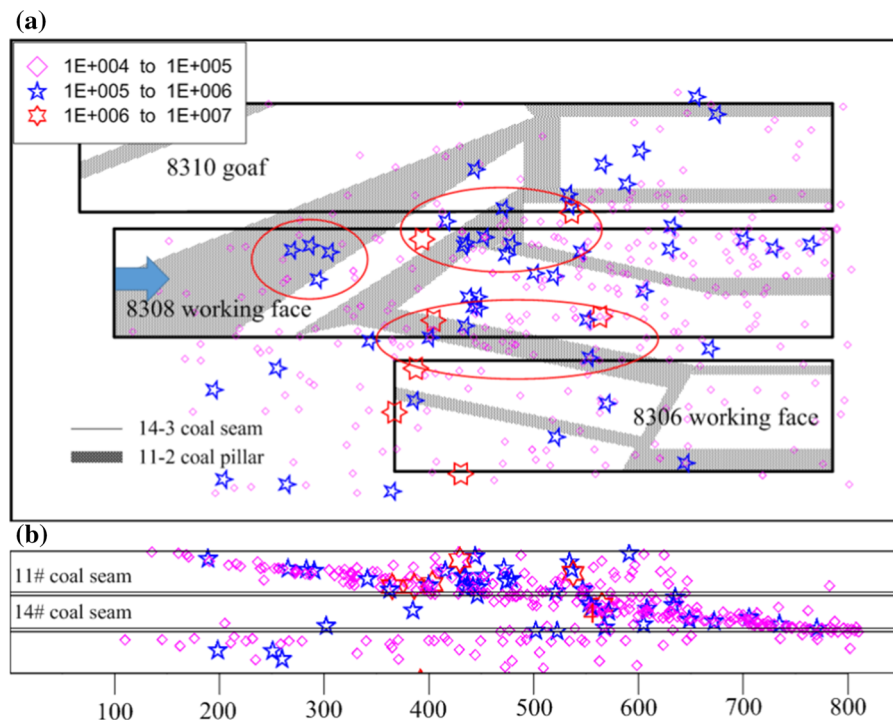
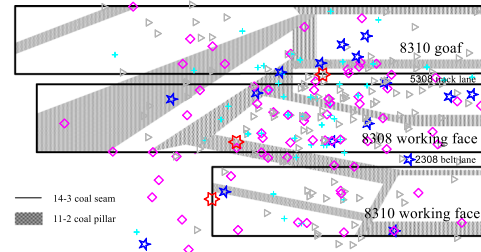
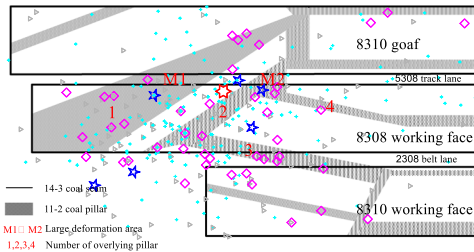


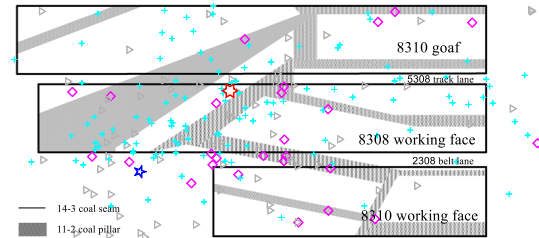
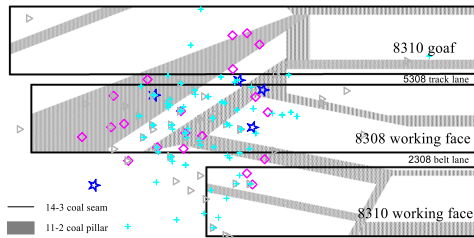
Fig. 4 a Distribution of microseismic events in horizontal section. b Distribution of microseismic events in vertical section

Table 2 Microseismic events on different layers

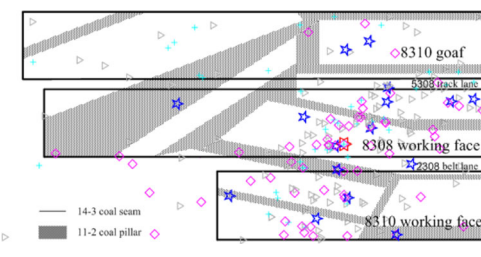
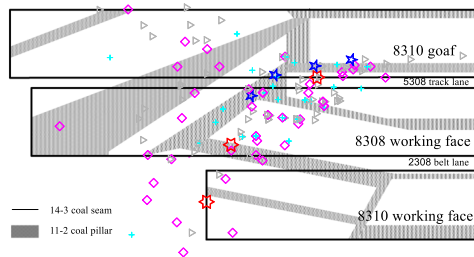
| Layers Energy (J) | 14-3 # Coal seam floor | 14-3 # Coal seam roof | 11-2 # Coal seam roof |
|---------------------------------|------------------------|-----------------------|-----------------------|
| $1 \times 10^4 - 1 \times 10^5$ | 60 | 147 | 130 |
| $1 \times 10^5 - 1 \times 10^6$ | 2 | 17 | 24 |
| $> 1 \times 10^6$ | 1 | 1 | 4 |



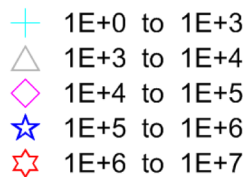
(a) Distribution of microseismic events during M1 mining (b) Distribution of microseismic events during M2 mining



(c) Spatial distribution of microseismic events in 11-2# coal seam and roof during M1 mining (d) Spatial distribution of microseismic events in 14-3# coal seam and roof during M1 mining



(e) Spatial distribution of microseismic events in 11-2# coal seam and roof during M2 advancing period (f) Spatial distribution of microseismic events in 14-3# coal seam and roof during M2 advancing period



(g) Mine seismic intensity classification

Fig. 5 Spatial distribution of microseismic events

the 8308 working face, it can be seen that the microseismic events were mostly distributed on the roadways near gob. During the M2 mining period, the same distribution law was observed. The microseismic events were mostly distributed in the M2 area of the mining position and the coal pillar area in front of the M2. Microseismic events on roadways near gob were significantly more than those on another side.

In summary, the spatial distribution law of above microseismic events has obvious zoning characteristics on the horizontal section, which is mainly concentrated under the coal pillars, especially at the junction of coal pillars on the side of the roadway near gob. On the striking profile, the microseismic events are mainly distributed in the vicinity of the coal pillars of the 14-3 and 11-2 # coal seam roofs. At the same time, the distribution of microseismic events also changes dynamically with the advancement of the working surface, which is predominately distributed in the range of 100 m in front of the working surface. There is a distinct correlation with the above-mentioned static stress concentration region.

3.2.2 Time Series Analysis of Microseismic Energy and Frequency

The accumulated energy, and frequency were selected as the indicators of microseismic time sequence law to analyze micro-seismic anomalous active area during the mining time. The analytic result can be used as verification and supplement of the dynamic disturbance risk zone to obtain the microseismic activity change under the overlying coal pillar. According to the statistical microseismic data of the entire mining period in the 8308 working face, the time series distribution curve of the accumulated energy, and frequency were obtained. Furthermore, the positions of the coal pillars in the roadways near gob entering M1 and M2 areas were compared and analyzed, as shown in Fig. 6.

Before the roadways near gob entered the M1 area, the frequency of microseismic energy remained at a low level. During the whole period from the entry of the M1 coal pillar to the exit of the M2 coal pillar, the microseismic energy and frequency entered a distinctly active state, in which the energy and frequency increased initially and then decreased. The maximum value of energy occurred in the area between the M1 and M2 coal pillars. These results indicated that when

the working face mined in the M1 and M2 areas, the roofs of the upper and lower coal seams were all active with increased energy and frequency. After the mining moved to the position of the coal pillar, the microseismic event entered a calm state.

4 Analysis of Large Deformation Mechanism of Roadway

4.1 Analysis of Static Load Stress Concentration Mechanism

According to the influence of both the overlying coal pillar and side abutment pressure on the static load stress concentration of the lower coal seam, the force model of the coal seam under the upper coal pillar was established, as shown in Fig. 7. A rectangular coordinate system was established with the O point as the coordinate origin. The x-axis was taken above the coal seam roof, and the positive direction of the y-axis was taken from the direction of the lower coal seam. Wherein, $M(x, y)$, $A(x_A, 0)$, $B(x_B, 0)$ represent any point on the lower coal seam, the left and right endpoints of any overlying coal pillar, respectively. $\bar{\sigma}_3$ refers to the stress received above the coal pillar or goaf. According to the theory of elastic mechanics, the vertical stress transmitted to the point M by the remaining coal pillars is as shown in Eq. (2):

$$\sigma_3 = -\frac{\bar{\sigma}_3}{\pi} \left[\arctan \frac{x-x_B}{y} - \arctan \frac{x-x_A}{y} + \frac{y(x-x_B)}{y^2+(x-x_B)^2} - \frac{y(x-x_A)}{y^2+(x-x_A)^2} \right] \quad (2)$$

Therefore, the total stress transmission of the upper coal pillar received by the M point is $\sigma_I = \sum \sigma_i$, $i = 1 \sim n$.

The side abutment pressure consists of 2 parts: the gravity stress σ_γ and the additional stress increment transmitted by the goaf $\Delta\sigma$, namely:

$$\sigma_{II} = \sigma_\gamma + \Delta\sigma \quad (3)$$

Thereby, the coal seam is subjected to the above total static stress transmission. $\sigma_j = \sigma_I + \sigma_{II}$.

According to the actual conditions of the working face, measure the width of overlying coal pillars, mined-out area and the distance between the upper and lower coal seams at the position of I-I in Fig. 2, and

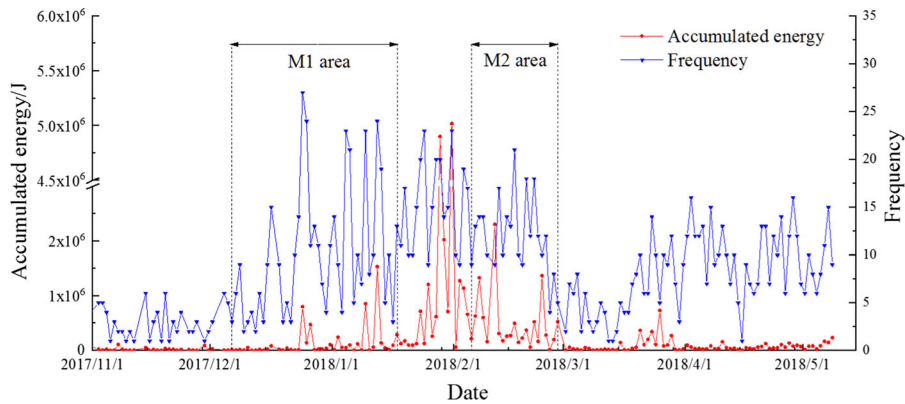


Fig. 6 Time serial variation of microseismic energy and frequency

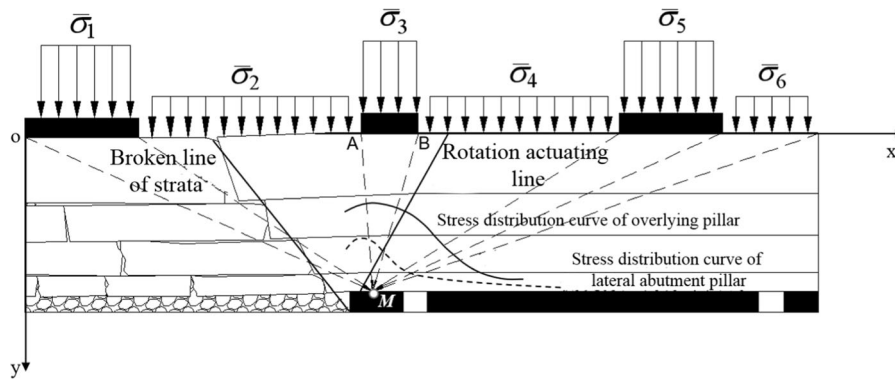


Fig. 7 Static stress concentration integrated stress model

then bring the measurement results into the upper coal seam stress transfer Eq. (2). Stress distribution curve of lateral abutment pillar can be calculated according to the calculation formula of side support pressure at the same time. Figure 7 shows the stress distribution curve transferred by the coal pillar above the 14-3 # coal seam and the stress distribution curve of lateral abutment pillar. The upper transfer stress and side abutment pressure of the overlying coal pillar at the I-I position are mainly concentrated on the side of the roadways near gob. When the working surface was advanced to the front of the coal pillar, the influence of the pilot support pressure was superimposed, and the static load stress concentration below the coal pillar reached the maximum value.

Combined with the above analysis of the seismic computed tomography CT inversion results, the stress concentration area is mostly distributed on the side of the roadway near goaf, which is consistent with the theoretical calculation results. When the mining was

about 100 m before the coal pillar, the positive anomaly coefficient of the wave velocity directly below the front coal pillar reached 0.1 or more. The positive anomaly coefficients of the wave velocity at the junction of the coal pillar 1, the coal pillar 2, and the temporary tunnel reached 0.2. The area where the coefficient reached 0.2 corresponded to the large deformation area of the roadway. As the working face advanced forward, the stress concentration area varied dynamically, which is consistent with the evolution law of the stress area of the advanced support. The comprehensive seismic computed tomography CT inversion and stress transfer calculation results showed that the large deformation zone of the roadway was affected by the stress transfer of the overlying coal pillar, the advanced abutment pressure, and the stress transfer of the cantilever roof in the lateral goaf.

4.2 Analysis of the Dynamic Disturbance Mechanism

During the mining process, there are many dynamic load damages, such as roof fracture, blasting, and coal cutting. Under the condition of mining coal pillars in close coal seams, in addition to the dynamic load caused by the fracture of the roof of the coal seam, the working face mining will lead to the instability of the remaining coal pillars in the upper layer and the secondary fracture of the roof, which causes dynamic load damage and spreads to the lower layer working face.

According to the theory of elastic wave propagation, the additional stress σ_d caused by the stress wave generated by vibration from the source to the coal and rock mass around the mining space is:

$$\sigma_d = \sigma_0 e^{-\lambda L} \quad (4)$$

In the equation, σ_0 , λ , and L represent the initial intensity of the stress wave generated by the vibration, the vibration wave energy attenuation index, and the distance from the source to the local position of the mining space, respectively.

The dynamic and static load superposition principle is shown in Fig. 8. The discriminant formula of the coal seam impact under the influence of dynamic and static load superposition is shown in equation

$$\sigma_j + \sigma_d \geq \sigma_{\min} \quad (5)$$

wherein σ_j and σ_{\min} represent the static load stress caused by the multi-force source and the critical stress when the rock burst occurs, respectively.

It can be seen from the above equation that the dynamic propagation damage attenuation is mainly affected by the source distance. The small coal seam spacing not only aggravates the mining surface impact of the overlying coal pillars and the roof but also increases the additional stress of the dynamic load damage. Therefore, under the conditions of mining coal pillars at close range, the degree of damage caused by the dynamic disturbance to the working surface cannot be ignored.

Through the spatial location analysis of the microseismic monitoring data, it was found that the microseismic events were mostly distributed in the vicinity of the coal pillars in the horizontal positioning map while the microseismic events were mainly

distributed in the 14-3 and 11-2 # coal seam roofs in the vertical section along the strike. At the same time, the mine earthquake events on the south side of the M2 area were mainly distributed in the 11-2 # coal seam roof, while the mine earthquake events on the north side of the M2 area were distributed in the 11-2 and 14-3 # coal seam roofs with a predominance in 14-3 # coal seam roof. This distribution feature indicated that due to the large size of the coal pillars 1 and 2, the roof plate was not fully fractured during the mining of the 11-2 # coal seam, and the secondary fracture of the 11-2 # coal seam roof during the mining of the 8308 working face through the coal pillars 1 and 2 was severe. After the mining of M2 area, only the coal pillar 4 was left above the 8308 working face with a small size. At this time, the 14-3 # coal seam roof was predominately fractured because the area was sufficiently fractured when mining the 11-2 # coal seam. This result indicated that the dynamic load disturbance was generated during the 14-3 # coal seam fracture under the influence of the coal pillar and the secondary fracture of the 11-2 # coal seam roof.

Through the spatial distribution of the microseismic events during the mining of the M1 and M2 areas and the time serial analysis of energy frequency, it was found that the microseismic events were mainly distributed in the vicinity of roadways near gob in front of the mining area, indicating that the spatial distribution of the microseismic events is also subject to the pilot support pressure and the side abutment pressure. The effect is consistent with the distribution of stress concentration areas. This result indicated that the dynamic load disturbance of 8308 working face exhibited a corresponding relationship with static load stress concentration. Comparative analysis of Figs. 3c and 4 indicated that the dynamic load disturbance with greater than 1×10^6 J energy occurred in the coal pillar 3 area. However, the positive velocity coefficient of the wave velocity in this area only reached 0.1 without large deformation of the roadway, indicating large deformation of the roadway in 8308 working face is dominated by static load stress.

The integration of the spatial distribution of microseismic with time serial analysis of energy frequency indicated that the roof structure was stable due to the large coal pillar 1. The roof structure continuously maintained a steady state of energy accumulation when the mining position was between

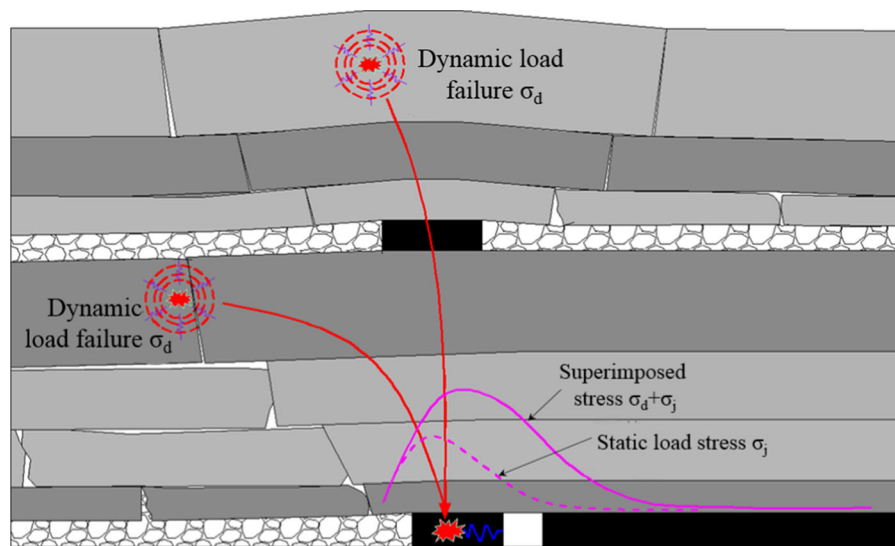


Fig. 8 Schematic diagram of dynamic load disturbance in close distance coal seam

entering coal pillar and the central region of the M1. When the mining position approached the exit of coal pillars, the roof continued to fracture, releasing a lot of energy. After the M1 area, due to the influence of the roof activity and the concentrated stress of the coal pillars 1 and 2, the microseismic event was active. After the mining position entered the coal pillar 2, since the coal pillar 2 across the entire working surface diagonally, the underside of the south side of the coal pillar 2 was hollowed out, causing the stress to continuously shift to the M2 area. In addition, the impact of the suspended roof causes the other side of the M2 area to be simultaneously destroyed. As the work progressed forward, the continuous fracture of the coal pillar 2 caused continuous destruction of the M2 area. When the M2 area was mined, it was almost completely fractured and stabilized again, and the microseismic event showed a downward trend. This trend indicated that the dynamic disturbance generated by the 8308 working face is mainly affected by the roof activity under the influence of coal pillars.

4.3 Analysis of Large Deformation Mechanism of Roadway

Based on the research results of the distribution law of large deformation area and static load stress concentration, as well as the dynamic load disturbance mechanism, the large deformation mechanism of 8308 working face roadway is as follows: large deformation

area of roadway M1 and M2 are located at the junction of large area overlying coal pillars with the roadway near goaf. During the mining process of the working face, the residual coal pillar of the 11-2 # coal seam transmits the stress to the roof and floor of the 14-3 # coal seam, which is superimposed with the lateral abutment pressure and the advanced abutment pressure of the 8308 working face to cause the static load stress concentration on the coal pillars in roadway near goaf. The stress concentration in the area generates the fracture of 14-3 # coal seam roof, the secondary fracture in 11-2 # coal seam roof, and dynamic load disturbance. The dynamic load disturbance area coincides with the static load stress concentration area, which causes a large deformation in the roadway near goaf. In particular, static load stress concentration is the main influencing factor.

When mining the lower coal seam with close multiple seams, it will be affected by many factors such as pressure relief, stress concentration, secondary dynamic load disturbance and so on. The stress concentration and dynamic load disturbance caused by the upper coal seam usually occur at the same time, so the rock burst induced by dynamic and static load superposition will not occur in the pressure relief area caused by the mining of the upper coal seam. In the stress concentration area caused by the upper coal seam, it is necessary to focus on monitoring the occurrence of rock burst, and guide the prevention and control of static stress concentration and dynamic load

disturbance according to the theory of dynamic and static superposition.

5 Conclusion

- (1) According to the seismic computed tomography, it was found that the high wave velocity region was consistent with the overlying pillar affecting zone. The wave velocity anomaly coefficient was as high as 0.2, indicating that the remaining coal pillar area has a higher static load stress concentration.
- (2) According to the data analysis of microseismic monitoring, the large-energy mine earthquakes ($> 10^4$ J) were mainly distributed in the vicinity of the roadway near goaf in front of the mining area under the coal pillar. On the vertical profile of the working face, these events were mainly distributed in the 14-3 and 11-2 # coal seam roofs. These results indicated that the roof fractured during the mining process of the 8308 working face and generated dynamic load disturbance, which is affected by the regional static load stress concentration.
- (3) The large local deformation of the roadway is due to the downward stress transfer of the coal pillars in the upper coal seam, which is superimposed with the lateral abutment pressure and the advanced abutment pressure to cause static load stress concentration in the roadway near goaf under the residual coal pillar. Under the influence of static load stress concentration and mining, the residual coal pillars and the roof of the top fractured and slipped to generate dynamic load disturbance. The superposition of dynamic load disturbance and static load concentrated stress caused large deformation of the roadway near goaf under the coal pillar, in which the static load stress concentration is the main influencing factor.
- (4) Under the condition of close multi-coal seam mining, the stress concentration and dynamic load disturbance caused by the upper coal seam usually occur at the same time and stress concentration and dynamic load disturbance usually do not occur under the goaf of the upper coal seam. Therefore, it is necessary to focus on

the area affected by the overlying pillars. The detection of static load stress and dynamic disturbance should be carried out at the same time to control and prevent large deformation.

Acknowledgements This work was financially supported by the National Natural Science Foundation of China (Grant No. 51634001, 51774023) and Beijing Science and Technology Nova Project (Grant No. xx2018073). The authors would like to express their gratitude to all the agencies for funding this research.

References

- Cai W, Dou L, Cao A et al (2014) Application of seismic velocity tomography in underground coal mines: a case study of Yima mining area, Henan, China. *J Appl Geophys* 109:140–149
- Cai Wu, Linming D, Zhenlei Li et al (2016) Verification of passive seismic velocity tomography in rock burst hazard assessment. *Chin J Geophys Chin Ed* 59(1):252–262
- Cao A, Dou L, Cai W et al (2015) Case study of seismic hazard assessment in underground coal mining using passive tomography. *Int J Rock Mech Min Sci* 78:1–9
- Cao A, Dou L, Cai W et al (2016) Tomographic imaging of high seismic activities in underground island long wall face. *Arab J Geosci* 9(3):1–10
- Cartwright PB (1997) A review of recent in-situ stress measurements in United Kingdom Coal Measures Strata. In: proceedings international symposium on rock stress, Kumamoto, Japan 469–474
- Chen X, Guo H, Zhao P et al (2011) Numerical modeling of large deformation and nonlinear frictional contact of excavation boundary of deep soft rock tunnel. *J Rock Mech Geotech Eng* 3:421–428
- Dou L, Cai W, Gong S et al (2014) Dynamic risk assessment of rock burst based on the technology of seismic computed tomography detection. *J China Coal Soc* 39(02):238–244
- Fuxing J, Xianfeng S, Cunwen W (2015) Mechanical mechanism of rock burst accidents in slice mining face under high pressure. *Chin J Geotech Eng* 37(6):1123–1131
- Fuxing J, Yuxiao W, Ming Li et al (2017) Mechanism of rockburst occurring in protected coal seam induced by coal pillar of protective coal seam. *Chin J Geotech Eng* 39(09):1689–1696
- Gao R, Yu B, Meng X (2019) Stress distribution and surrounding rock control of mining near to the overlying coal pillar in the working face. *Int J Min Sci Technol* 29(6):70–76
- Han L, Qiao W et al (2013) The deformation failure mechanism and control techniques of soft rock in deep roadways in Zhaolou mining. *J Min Saf Eng* 30(02):165–172
- He X, Anhu W, linming D et al (2018) Technology of micro-seismic dynamic monitoring on coal and gas outburst-prone zone. *J China Coal Soc* 43(11):3122–3129
- Hosseini N, Oraee K, Shahriar K et al (2012) Passive seismic velocity tomography on longwall mining panel based on

- simultaneous iterative reconstructive technique. *J Cent South Univ* 19(08):2297–2306
- Jinfeng J, Jialin X, Weibing Z et al (2010) Mechanism of strong strata hazards during the working faceout of the upper dip coal pillar in contiguous seams. *Chin J Geotech Eng* 35(01):15–20
- Junfeng P, Shuwen W, Shaohong L (2014) Pre-evaluation of burst hazards based concentrated static load detection. *Chin J Geotech Eng* 36(7):1227–1234
- Li G, Ma F, Guo J et al (2020) Study on deformation failure mechanism and support technology of deep soft rock roadway. *Eng Geol* 264(C)
- Li SC, Wang Q, Wang HT et al (2015) Model test study on surrounding rock deformation and failure mechanisms of deep roadways with thick top coal. *Tunn Undergr Space Technol* 47:52–63
- Li X, Gong F, Tao M et al (2017) Failure mechanism and coupled static-dynamic loading theory in deep hard rock mining: a review. *J Rock Mech Geotech Eng* 9(4):767–782
- Li ZL, He XQ, Dou LM et al (2018) Rockburst occurrences and microseismicity in a longwall panel experiencing frequent rockbursts. *Geosci J* 22(4):623–639
- Liu C (2018) Research on deep-buried roadway surrounding rock stability and control technology. *Geotech Geol Eng* 36(6):3871–3878
- Mark C, Chase FE, Pappas DM (2007) Analysis of multiple seam stability. In: proceedings of the 26th international conference on ground control in Mining, 5–18
- Qing-bin MENG, Li-jun HAN, Wei-guo QIAO et al (2013) The deformation failure mechanism and control techniques of soft rock in deep roadways in Zhaolou mining. *J Min Saf Eng* 30(02):165–172
- Sun Y, Zuo J, Karakus M et al (2019) Investigation of movement and damage of integral overburden during shallow coal seam mining. *Int J Rock Mech Min Sci* 117:63–75
- Tulu IB, Esterhuizen GS, Gearhart D et al (2018) Analysis of global and local stress changes in a long wall gate road. *Int J Min Sci Technol* 28(1):127–135
- Wang C, Jiang F, Wang P et al (2009) Microseismic events distribution characteristics and mechanical mechanisms of rock bursting induced by a coal pillar. *J China Coal Soc* 34(9):1169–1173
- Wang Q, Pan R, Jiang B et al (2017) Study on failure mechanism of roadway with soft rock in deep coal mine and confined concrete support system. *Eng Fail Anal* 81:155–177
- Yan H, Hu B, Xu T (2012) Study on the supporting and repairing technologies for difficult roadways with large deformation in coal mines. *Energy Procedia* 14:1653–1658
- Yang X, Pang J, Liu D et al (2013) Deformation mechanism of roadways in deep soft rock at Hegang Xing'an Coal Mine. *Int J Min Sci Technol* 23(2):307–312
- Yang SQ, Chen M, Jing HW et al (2017) A case study on large deformation failure mechanism of deep soft rock roadway in Xin'an coal mine. *China Eng Geol* 217:89–101
- Zhao J, Liu L, Zheng Z (2018) Law of strata pressure behavior in shallow coal seam. *IOP conference series: earth and environmental science* IOP Publishing 113(1):012011
- Zhu W, Xu J, Li Y (2017) Mechanism of the dynamic pressure caused by the instability of upper chamber coal pillars in Shendong coalfield. *China Geosci J* 21(5):729–741

Publisher's Note Springer Nature remains neutral with regard to jurisdictional claims in published maps and institutional affiliations.